Copy 216

RM A53D29

NACA

RESEARCH MEMORANDUM

PERFORMANCE OF A NORMAL-SHOCK SCOOP INLET WITH BOUNDARY-LAYER CONTROL

By Alson C. Frazer and Warren E. Anderson

Ames Aeronautical Laboratory
Moffett Field, Calif.

NATIONAL ADVISORY COMMITTEE
FOR AERONAUTICS

WASHINGTON

June 29, 1953

NATIONAL ADVISORY COMMITTEE FOR AERONAUTICS

RESEARCH MEMORANDUM

PERFORMANCE OF A NORMAL-SHOCK SCOOP INLET WITH BOUNDARY-LAYER CONTROL

By Alson C. Frazer and Warren E. Anderson

SUMMARY

Tests were made on a normal-shock inlet mounted as a scoop on a flat plate on which a turbulent boundary layer was generated. A boundary-layer-removal scoop was provided between the inlet and the plate and various amounts of the boundary layer were removed. The effect of partial boundary-layer admittance to the main inlet on the total-pressure recovery and flow stability was determined over a range of free-stream Mach numbers from 1.35 to 1.75 and a range of scoop mass-flow ratios from maximum to the least for which stable flow could be maintained.

Results of the tests indicated that the inlet flow stability was unsatisfactory when the boundary-layer scoop was located in the entrance plane of the main inlet; the stability was markedly improved when the boundary-layer scoop was extended upstream. The total-pressure recovery of the main inlet increased with boundary-layer removal for all Mach numbers. Thrust calculations, which included calculated cowl, additive, and boundary-layer-removal drags, indicated an optimum boundary-layer removal of approximately 70 percent of the total boundary-layer thickness for all mass-flow ratios and inlet Mach numbers tested. Comparison of the thrust of the scoop inlet with the thrust that would be available if normal-shock pressure recovery and no boundary-layer-removal drag had been realized indicated that the scoop system can develop from 96 to 100 percent of this idealized thrust when optimum boundary-layer removal is used.

INTRODUCTION

In the design of jet-propelled aircraft it is often desirable to locate the air inlets aft along the fuselage. Such inlet locations involve the problem of fuselage boundary layer and its influence on the inlet performance. In general, the admittance of this boundary layer

into a normal-shock scoop-type inlet results in a reduction in the diffuser flow stability at reduced mass-flow ratios and also in a loss in the total-pressure recovery. For supersonic inlet velocities these adverse effects are increased due to shock-wave boundary-layer interactions. The inlet characteristics can be improved if the boundary layer ahead of the inlet is removed. However, boundary-layer removal causes drag, the magnitude of which must be compared with the increase in thrust resulting from the improved pressure recovery. Such an evaluation requires knowledge of the relationship between the removal drag and the thrust obtained by use of the main inlet with boundary-layer removal.

The effect of boundary-layer removal on the total-pressure recovery and flow stability of a half conical-shock side-scoop inlet has been previously reported. For example, references 1 and 2 indicate large improvements may be had in both of these characteristics. Several inlets utilizing a variety of external compression surfaces are compared in reference 3, but for the condition of complete boundary-layer removal only.

The purpose of the present tests was to determine the optimum amount of the total boundary-layer thickness to be removed forward of a normal-shock scoop inlet for the attainment of the maximum net thrust and the attainment of a broad range of stable mass-flow ratios at all Mach numbers. The model used was a normal-shock scoop inlet which can be expected to have high net internal-thrust coefficients at Mach numbers up to about 1.5 according to calculations reported in reference 4. All inlet characteristics required for calculation of the net thrust were measured over the Mach number range from 1.35 to 1.75.

SYMBOLS

A	area, sq ft
$(C_{F_N})_P$	$C_{F_N}'\left(\frac{m_1}{m_0}\right)\left(\frac{A_1}{S_P}\right)$, coefficient of net thrust based on S_P, dimensionless (See Appendix.)
$(C_{F_N})_{P_{ideal}}$	ideal net thrust coefficient based on S_P (assumes normal-shock-wave total-pressure recovery and no boundary-layer-removal drag), dimensionless
d	distance measured positive in the upstream direction from the inlet station, in.
H	total pressure, lb/sq ft
h	height of boundary-layer scoop, in.

$H_{B.L.o}$	$\frac{\delta}{h}\int_o^{h/\delta} H_l \, d\left(\frac{y}{\delta}\right)$
H_l	local total pressure within the boundary layer, lb/sq ft
$H_{B.L.o}'$	$\frac{\delta}{h}\int_o^{h/\delta} H_l' \, d\left(\frac{y}{\delta}\right)$
H_l'	local total pressure following a normal shock at the local Mach number within the boundary layer, lb/sq ft
L	length of main scoop, in. (See fig. 1.)
M	Mach number, dimensionless
m	mass flow, slugs/sec
$\frac{m_1}{m_o}$	mass-flow ratio, $\frac{\rho_1 V_1 A_1}{\rho_o V_o A_1}$
p	static pressure, lb/sq ft
r	radius of internal scoop contour, in.
S_p	engine frontal area, sq ft
U	local velocity immediately outside boundary layer, ft/sec
u	local velocity within the boundary layer, ft/sec
V	velocity, ft/sec
x	distance measured from the main inlet station, positive in the downstream direction, in.
y	distance measured normal to the mounting plate, in.
δ	boundary-layer thickness ($\frac{u}{U} = 0.99$), in.
ρ	mass density, slugs/cu ft

Subscripts

o	flow conditions on the mounting plate forward of the boundary-layer scoop (referred to as free stream)

1	inlet station
3	diffuser total-pressure measuring station
e	exit station
B.L.	boundary layer

TEST APPARATUS

Wind Tunnel

The tests were performed in the Ames 8- by 8-inch supersonic wind tunnel. The test Mach number was varied by means of a sliding wall of the tunnel which results in a variable-throat area while maintaining a fixed test-section area. (See ref. 5.) The Reynolds number per foot varied from 7 to 11 million. Auxiliary vacuum pumps were employed to induce the mass flow into the main and boundary-layer scoops.

Model

A sketch of the model employed in these tests is shown in figure 1, and photographs of the models installed on the ceiling of the 8- by 8-inch supersonic wind tunnel are shown in figure 2.

The model consisted of three parts: (1) The semicircular, sharp-lip main inlet and diffuser; (2) a "boundary plate" which made up the upper surface of the main-inlet diffuser and also contained three sides of a narrow, rectangular, sharp-lip, boundary-layer scoop; and (3) a mounting plate over which a simulated fuselage boundary layer was generated. Two boundary-layer-scoop designs were tested as shown in the photographs.

A subsonic diffuser was designed to provide a local static-pressure gradient proportional to the local static pressure according to the method outlined in reference 6. The Mach number at the diffuser entrance was chosen as 0.70 which corresponds to the subsonic Mach number following a normal shock wave at a free-stream Mach number of 1.5. The terminal Mach number at the diffuser exit was chosen to be 0.50. The resulting variation of diffuser cross-sectional area is shown in figure 3. Very gradual diffusion is indicated for values of x/L from 0 to 0.2, corresponding to the diffusion rate that would result from a $1/2^{\circ}$ conical expansion. It was expected that this gradual initial area variation would be helpful in maintaining stable inlet flow under conditions of appreciable boundary-layer admittance to the main inlet. The advisability

of maintaining a very gradual rate of diffusion near the inlet as regards internal flow stability has been reported in reference 7. The subsequent diffusion rate is also gradual, being less than that for a 1° conical expansion up to an x/L value of approximately 0.90.

The boundary-layer-scoop diffusion was accomplished by a divergence of 3° between the upper-and lower surfaces of the duct. The duct side walls were parallel. Figure 2 shows the two positions of the boundary-layer-scoop leading edge which were tested. In figure 2(a) the boundary-layer scoop is located in the plane of the main inlet, and in figure 2(b) the boundary-layer scoop is located upstream of the main inlet a distance equal to 30 percent of the main-inlet radius. The height of the boundary-layer scoop was varied by introducing shims of various thicknesses between the mounting plate and the boundary plate.

The mounting plate extended 6 inches upstream of the main inlet and spanned the tunnel. To vary the boundary-layer thickness, trip wires were mounted spanwise on the mounting plate near the leading edge. The diameters of the trip wires ranged from 0.006 to 0.050 inch.

Instrumentation

The principal instrumentation consisted of total-pressure tubes located in the diffusers of the main and boundary-layer scoops, calibrated orifice meters, and internal static-pressure orifices located along the main-inlet diffuser. In addition, several total-pressure tubes were installed for reference purposes in the plane of the inlet and were used to assure repeatability of the boundary-layer profiles and the free-stream total pressure. These reference tubes, together with a number of static-pressure reference orifices on the mounting plate, are indicated in figure 1. Preliminary surveys were made on the mounting plate before the boundary plate and diffuser were installed. These preliminary tests were conducted using separate total- and static-pressure rakes to obtain data at the inlet station for the calculation of the boundary-layer profiles and for the determination of the slight variation of the free-stream pressures due to the presence of the trip wires.

TEST PROCEDURE

The boundary-layer parameter, h/δ, was fixed by selecting values of scoop height and boundary-layer thickness. For values of $(h/\delta) > 0.67$, h was held constant (0.100 in.) and a trip wire to give the desired δ was chosen from the boundary-layer-profile data obtained in the preliminary tests. For $(h/\delta) < 0.67$, δ was held constant (0.150 in.) and h was varied

by the use of shims located between the boundary plate and the mounting plate. The main inlet was then operated over the stable range of mass-flow ratios at each test Mach number. The boundary-layer scoop was operated at all times at the greatest total-pressure recovery for the maximum possible mass-flow ratio.

ACCURACY

The accuracy of the data was estimated by considering the scatter of the data for repeated runs, the manometer lag and reading error, and the statistical probability error where multiple terms are involved in the definitions of a particular parameter. Estimates of the probable error in the data thus obtained are summarized in the following table:

Parameter	Percent probable error
H_3/H_0	±0.5
m_1/m_0	±1.0
$m_{B.L.}/m_0$	±1.0
$(C_{F_N})_P$	±1.5
M_0	±1.0
h/δ	±1.0

RESULTS AND DISCUSSION

The total boundary-layer thicknesses and velocity profiles for the various trip wires which were employed are shown in figure 4. The velocity profile which corresponds to the seventh-power law of turbulent boundary layers is also indicated. The effect of Mach number on both the total thickness and profile shape was very small and within the experimental accuracy of the measurements.

Initial tests were conducted with the boundary-layer scoop located in the plane of the entrance to the main inlet (see fig. 2(a)). It was observed, however, that the internal flow became unstable at mass-flow ratios slightly less than unity for all values of Mach number and h/δ. The model was therefore modified as shown in figure 2(b) in an attempt to improve the flow stability. The modification, which consisted of locating the boundary-layer scoop upstream of the main inlet scoop a distance equal to 30 percent of the main inlet radius, was successful and all data and discussion presented in this report pertain to the modified model.

Main Inlet

Visual flow observation.- An extensive study of the schlieren pictures, which were taken of the external-flow patterns for all test conditions, was made in order that an empirical relationship could be determined between the main-inlet mass-flow ratio, free-stream Mach number, and main-inlet normal-shock-wave position. Since the boundary-plate extension can be considered to be a design variable, depending upon Mach number and the range of subcritical mass-flow ratios to be encountered (subcritical refers to mass-flow ratios less than maximum), such a relationship was considered to be pertinent to the test results. The results of the study are shown in figure 5 by curves which represent the average for all values of h/δ. A straight line at $d/r_1 = 0.30$ represents the extension of the boundary plate arbitrarily selected for use in the present tests. Also deduced from the study of the schlieren pictures were typical external-flow patterns which are presented in figure 6 and which will be helpful in clarifying some of the results presented in later paragraphs. The external flow was observed to vary primarily with mass-flow ratio and h/δ. The effect of Mach number was to influence the terminal upstream position of the main-inlet normal shock for which stable internal flow could be maintained.

Total-pressure recovery.- The variations of the main-inlet total-pressure recovery with mass-flow ratio for various values of free-stream Mach number and h/δ are shown in figure 7. The free-stream Mach numbers were slightly different, due to shock waves which were generated by the boundary-layer trip wires. The data are presented for the range of stable mass-flow ratios and show that the total-pressure recovery increased as the mass-flow ratio decreased at all Mach numbers for test values of h/δ greater than zero. A secondary increase in recovery was noted at a reduced mass-flow ratio for many test conditions. This secondary rise in total pressure was due to the external-flow pattern that existed when the normal shock wave was located upstream of the boundary-layer scoop. The schlieren pictures of the flow reveal that the boundary layer upstream of the boundary-layer scoop thickened or separated when the normal shock wave impinged upon it. This thickening or separation resulted in shock-wave bifurcation. The suction which was applied to the boundary-layer scoop succeeded in turning the thickened or separated flow back toward the scoop which captured all or part of it, depending upon the particular value of h/δ and m_1/m_0. Under this condition, the main inlet realized a two-shock pressure recovery over a small part of the inlet area, which resulted in a secondary gain in the total-pressure recovery. In order to correlate the occurrence of the secondary gain in total-pressure recovery with the shock-wave location upstream of the boundary-layer scoop, a dashed line is shown in the figures to indicate the mass-flow ratio - Mach number relationship that existed when the shock wave was located at the leading edge of the boundary-plate extension. A secondary rise is not always indicated

since, for h/δ less than 1.0, some of the boundary-layer flows into the main inlet and the external main-inlet normal shock wave may bifurcate when located on the boundary plate. Under these conditions, the secondary gain is replaced by a uniform rise in pressure recovery throughout the range of subcritical mass-flow ratios. At low values of h/δ the large amount of boundary layer going into the main inlet completely eliminated the secondary increase in pressure recovery. Instead, unstable flow resulted with a consequent drop in the total-pressure ratio.

The data of figure 7 were cross-plotted against h/δ for several selected Mach numbers at a mass-flow ratio of 0.95 and are shown in figure 8. The variation in the experimental free-stream Mach numbers over the range of h/δ made it necessary to interpolate for the selected values of the Mach number. Also shown in figure 8 are curves which represent a theoretical maximum total-pressure recovery. These curves were obtained by integrating normal-shock-wave total-pressure recovery at the measured local Mach number across the plane of the entrance to the inlet and through the boundary layer. Good agreement was obtained between these results and those calculated by the method of reference 8. An additional allowance was made for an internal loss equal to 2 percent of the subsonic dynamic pressure at the entrance. Such a loss is believed to be reasonable for the diffuser used in this investigation. The difference between the experimental and the theoretical curves represents the effect of the boundary layer on the subsonic diffusion process. The principal gain in total-pressure recovery resulting from boundary-layer removal is seen to occur at low values of h/δ. The over-all improvement in total-pressure recovery due to boundary-layer removal ranged from 6 to 8 percent of the free-stream total pressure over the entire range of Mach numbers tested. This improvement is considerably less than that which was reported in reference 1, which may be due, in part, to the difference in methods of external compression and in subsonic diffuser design between the two tests. In reference 1 an external compression surface was utilized and, also, larger adverse pressure gradients existed within the subsonic diffuser. Both of these factors bring about reduced pressure recovery in the presence of boundary layer and, therefore, boundary-layer removal could be expected to result in a greater percent improvement for the inlet of reference 1 than for that of the present investigation.

Flow stability.- The internal flow in the main inlet was observed to be stable over a range of subcritical mass-flow ratios which generally decreased with an increase in Mach number and/or a decrease in h/δ. (See fig. 7.) For the lower two nominal Mach numbers tested (1.35 and 1.47), the lowest stable mass-flow ratios were such that the main-inlet normal shock wave was located considerably forward of the leading edge of the boundary-layer scoop for all values of h/δ other than $h/\delta = 0$. This was also true at a Mach number of 1.65 for all values of $(h/\delta) > 0.42$. At the highest test Mach number ($M_o = 1.77$), unstable flow occurred at $(h/\delta) < 0.69$ with the normal shock located on the boundary plate. The

ability of the main inlet to maintain stable internal flow with large amounts of boundary layer admitted to the duct may be attributed to the low static-pressure gradients in the subsonic diffuser. The importance of the subsonic-diffuser design on the stability characteristics of an inlet has been reported previously in references 6 and 9.

Internal pressure distribution.- The variation of static pressure along the intersection of the plane of symmetry with the surfaces of the subsonic diffuser is indicated in figure 9 for representative mass-flow ratios at extreme values of h/δ and free-stream Mach numbers. The two curves at $(m_1/m_0) = 1.0$ represent two normal-shock-wave locations within the duct. The agreement of the pressures measured on the opposite surfaces of the duct indicate that the diffusion was uniform, a conclusion which was supported by the total-pressure contours at station 3 which were obtained with the total-pressure rake. Each test condition, with a single exception, resulted in a symmetrical total-pressure distribution with a high-pressure central region which increased in size with an increase in h/δ. The exception noted was for a value of h/δ of zero and a Mach number of 1.77 with the main-inlet normal shock wave located inside the diffuser. For this test point a slight asymmetry of flow was detected, due to flow reversal in the vicinity of the duct corners.

Boundary-Layer Scoop

Total-pressure recovery.- In order to evaluate properly the efficiency of the boundary-layer-removal system, it was first necessary to determine the average available total pressure at the entrance of the boundary-layer scoop. Therefore, calculations were made, based on the measured boundary-layer velocity profiles and also on the theoretical turbulent-velocity profile. The ratio of the average available total pressure to the free-stream total pressure is presented for both the measured and theoretical profiles in figure 10 as a function of h/δ. The measured data, shown for Mach numbers approximately equal to 1.35 and 1.75, show good agreement with the theoretical predictions and represent the maximum total pressure that could be recovered within the boundary-layer scoop under conditions of isentropic compression.

Figure 11 shows the ratio of the actual total-pressure recovery that was attained to that which was theoretically available. The efficiency of the diffuser in recovering the available total pressure was less than 0.86 for all test conditions and decreased as h/δ increased beyond 0.5. The effect of Mach number was small. Also shown in the figure are curves which represent the ratio of the integration of the normal-shock total-pressure recoveries across the scoop entrance to the available total pressure. In the calculation of these curves, the total pressure and Mach number profiles within the boundary layer were used,

and the normal-shock total-pressure ratio was based on the local Mach number. The difference between the curves for the same Mach number represents a measure of total-pressure-ratio gain that might be realized with a more efficient boundary-layer diffuser. Additional research on the flow of boundary layer in scoops is required if higher total-pressure recovery and, consequently, lower boundary-layer-removal drag, are to be realized.

Mass flow.- The ratio of the maximum boundary-layer-scoop mass flow to the maximum main-inlet mass flow is shown in figure 12 as a function of h/δ for the highest and lowest Mach numbers tested. The effect of Mach number is seen to be small, while the effect of increasing h/δ is large for $(h/\delta) < 0.6$, but thereafter the effect decreases. The variation is probably due to the relatively small change in the velocity profile which results from a change in δ when h/δ is near 1.0. For h/δ less than 0.6, the amount of boundary-layer-scoop flow was reduced by reason of the lower average velocities in the boundary-layer profile and the reduced inlet area. The ratio of measured mass flow to the theoretical maximum value based on the integration of the velocity profiles is shown in figure 13 as a function of h/δ for the two extreme values of Mach number which were tested and with the main inlet operating supercritically. For the highest test value of free-stream Mach number, the mass-flow ratio varied from values greater than 1.0 at the lowest h/δ tested to less than 1.0 at the higher h/δ. For the lowest Mach number, the mass-flow ratio was less than 1.0 over the entire range of h/δ. An explanation for the mass-flow ratios greater than 1.0 is probably that at low values of h/δ, the flow entering the boundary-layer scoop was subsonic. This being the case, the suction pressures could be transmitted upstream to affect the velocity profile, thereby allowing the increase in mass-flow ratio. The apparent mass-flow spillage at the higher h/δ may be due to local shock-wave detachment in the vicinity of the boundary-layer-scoop lips and side walls.

Evaluation of Results

In order to evaluate the worth of a boundary-layer-removal system, it is necessary to consider the net propulsive thrust of an installation which includes the drag associated with boundary-layer removal. The method for calculating internal thrust coefficients reported in reference 10 was used. This method makes possible rapid computation of the internal thrust coefficients as a function of total-pressure recovery and Mach number. The thermodynamic cycle of the turbojet engine used in the illustrative example contained in the reference report was assumed, and the calculations are based on engine operation with afterburner at an altitude above 35,000 feet. External cowl and additive drags were computed by the methods reported in references 11 and 12, respectively.

Boundary-layer-removal drag was computed by evaluating the change in the total momentum from the scoop inlet to an assumed exit where the exit static pressure was equal to that of the free stream. Isentropic flow was assumed to exist between the total-pressure-rake station and the fictitious exit. No attempt was made to correct for the drag that might result from the ejection of the flow into the free stream. All thrusts and drags were converted to coefficients which were based on the free-stream dynamic pressure and the assumed engine frontal area, S_p (see Appendix).

Figure 14 shows the relative increase in net propulsive thrust coefficient, $(C_{F_N})_P$, which may be obtained by the use of boundary-layer removal. The reference thrust coefficient is that which would be obtained with no boundary-layer removal. The results shown in this figure indicate that an increase in thrust can be obtained at all main-inlet mass-flow ratios and that a peak value is obtained at a value of h/δ of approximately 0.70. Figure 14 represents the results obtained at a free-stream Mach number of 1.34; identical trends were noted for all Mach numbers tested. It should again be mentioned that the test procedure required a change in δ for changes in h/δ near 1.0. As a result, δ/r_1 varied from about 0.076 to 0.120 which may have had an effect on the value of h/δ for peak thrust. Reference 1, however, shows the effect to be small for approximately the same range in δ/r_1.

Since the optimum value of the boundary-layer-removal parameter, h/δ, was observed to be 0.70 for all mass-flow ratios and Mach numbers, the relative increase in thrust for a test value of h/δ near the optimum ($h/\delta = 0.69$) was plotted as a function of inlet Mach number and inlet mass-flow ratio. The resulting curves are presented in figure 15. The effectiveness of boundary-layer removal in terms of net thrust apparently increases with Mach number, at least over the Mach number range tested. The effect of reducing the mass-flow ratio is to increase the thrust gain over the thrust that would be available under a condition of no boundary-layer removal. This mass-flow-ratio effect on the thrust increase is not due as much to the subcritical thrust increase of the inlet with boundary-layer removal as it is due to the sharp reduction in available thrust of the inlet not incorporating boundary-layer removal. The line of short dashes drawn on the figure indicates the boundary between the data which were obtained with the external normal shock wave located upstream of the boundary-layer scoop and those which were obtained with the shock wave located downstream of the boundary-layer scoop.

The comparison of the net propulsive thrust coefficients obtainable with the scoop inlet with optimum boundary-layer removal and the net propulsive thrust coefficients which would be obtainable if normal shock total-pressure recovery and no boundary-layer-removal drag existed is presented in figure 16 for several mass-flow ratios and over the range of test Mach numbers. The scoop inlet of the present tests is seen to

produce thrust coefficients from 96 to 100 percent of the value which would be obtained under the conditions assumed for the mass-flow ratios which would exist with the normal shock wave located on the boundary plate.

All the thrust calculations are considered to represent a trend that is likely to occur with boundary-layer control of the type investigated. However, the over-all performance of the boundary-layer-removal system and the optimum value of h/δ may be altered by a more judicious design of the boundary-layer-scoop diffuser and a different boundary-plate extension.

It appears evident from these tests and calculations that the net thrust coefficient of a normal-shock-type scoop inlet incorporating a boundary-layer-removal system may be very nearly equal to that of an ideal-normal-shock nose inlet.

CONCLUSIONS

An investigation of the effects of a turbulent boundary layer on the performance of a normal-shock scoop inlet at Mach numbers from 1.35 to 1.75 has led to the following conclusions:

1. An increase in the stable range of subcritical mass-flow ratio can be obtained for a normal-shock scoop inlet by extending the boundary-layer-removal scoop forward of the main inlet.

2. At all Mach numbers and mass-flow ratios tested, the maximum gain in net thrust occurred at a value of boundary-layer-scoop height equal to approximately 70 percent of the boundary-layer thickness.

3. Thrust comparison between the scoop inlet of the present tests incorporating optimum boundary-layer removal and an ideal normal-shock nose inlet indicated that the scoop-inlet thrust coefficients were from 96 to 100 percent of that of the idealized inlet over the Mach number range tested.

4. The flow in boundary-layer-removal scoops warrants additional investigation for the purpose of improving the pressure recovery and increasing the ratio of mass flow to that which is theoretically possible.

Ames Aeronautical Laboratory
National Advisory Committee for Aeronautics
Moffett Field, Calif.

APPENDIX

NET THRUST COEFFICIENT

The net thrust, as defined in reference 10, is

$$F_N = F_i - D_E$$

With the use of ΔM to denote the change in total momentum of the stream tube entering the inlet, the internal net thrust F_i becomes

$$F_i = \Delta M_{o-1} + \Delta M_{1-e} = \Delta M_{o-e}$$

Values of F_i can be obtained from reference 10. For the external drag

$$D_E = \Delta M_{o-1} + D_C + D_{B.L.}$$

The momentum term ΔM_{o-1} is the additive drag as discussed in reference 12 and is denoted by D_a. The values D_C and $D_{B.L.}$ are the drags due to the cowl pressure and the boundary-layer scoop, respectively. Therefore, by use of the coefficient notation of reference 10, the net thrust coeficient referred to A_o is

$$C_{F_N}' = C_{F_i}' - \left[C_{D_a}' + C_{D_C}' + C_{D_{B.L.}}' \right] = \frac{F_N}{q_o A_o}$$

The net thrust coefficient referred to S_P is then

$$(C_{F_N})_P = \frac{F_N}{q_o A_o} \times \frac{A_o}{S_P}$$

Unidimensionally

$$A_o = \frac{m_1}{m_o} A_1$$

Finally

$$(C_{F_N})_P = C_{F_N}' \times \frac{m_1}{m_o} \times \frac{A_1}{S_P}$$

[redacted]

REFERENCES

1. Goelzer, Fred H., and Cortright, Edgar M., Jr.: Investigation at Mach Number 1.88 of Half of a Conical-Spike Diffuser Mounted as a Side Inlet with Boundary-Layer Control. NACA RM E51G06, 1951.

2. Obery, Leonard J., Englert, Gerald W., and Nussdorfer, Theodore J., Jr: Pressure Recovery, Drag, and Subcritical Stability Characteristics of Conical Supersonic Diffusers with Boundary-Layer Removal. NACA RM E51H29, 1952.

3. Weinstein, M. I.: Performance of Supersonic Scoop Inlets. NACA RM E52A22, 1952.

4. Blackaby, James R.: An Analytical Study of the Comparative Performance of Four Air-Induction Systems for Turbojet-Powered Airplanes Designed to Operate at Mach numbers up to 1.5. NACA RM A52C14, 1952.

5. Allen, H. Julian: The Asymmetric Adjustable Supersonic Nozzle for Wind-Tunnel Application. NACA TN 2919, 1953. (Supersedes NACA RM A8E17)

6. Davis, Wallace F., Edwards, Sherman S., and Brajnikoff, George B.: Experimental Investigation at Supersonic Speeds of Twin-Scoop Duct Inlets of Equal Area. IV - Some Effects of Internal Duct Shape Upon an Inlet Enclosing 37.2 Percent of the Forebody Circumference. NACA RM A9A31, 1949.

7. Kantrowitz, Arthur R: The Formation and Stability of Normal Shock Waves in Channel Flows. NACA TN 1225, 1947.

8. McLafferty, George: Theoretical Pressure Recovery Through a Normal Shock in a Duct With Initial Boundary Layer. Jour. Aero. Sci., vol. 20, no. 3, Mar. 1953.

9. Allen, J. L., and Beke, Andrew: Force and Pressure-Recovery Characteristics of a Conical-Type Nose Inlet Operating at Mach Numbers of 1.6 to 2.0 and at Angles of Attack of 9°. NACA RM E52I30, 1952.

10. Brajnikoff, George B.: Method and Graphs for the Evaluation of Air-Induction Systems. NACA TN 2697, 1952.

11. Warren, C. H. E., and Gunn, R. E. W.: Estimation of External Drag of an Axially Symmetric Conical Nose Entry for Jet Engine at Supersonic Speeds. British TN No. Aero. 1934, S. D. 66, 1948.

12. Sibulkin, Marwin: Theoretical and Experimental Investigation of Additive Drag. NACA RM E51B13, 1951.

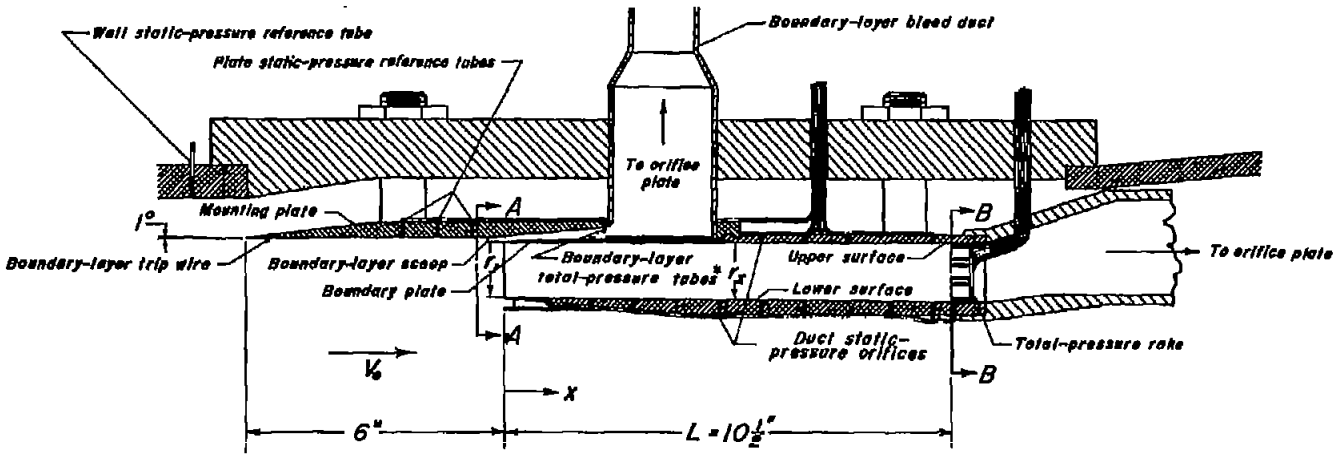

* Two tubes were spaced equidistant from the side walls

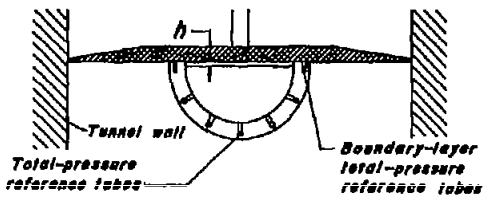

Section A-A

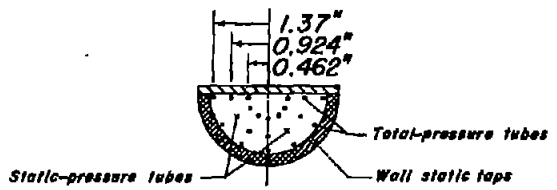

Section B-B

Duct coordinates (inches)

r_x	x	r_x	x	r_x	x
1.250	0.000	1.267	2.000	1.338	8.000
1.254	0.500	1.276	3.000	1.374	18.000
1.258	1.000	1.286	4.000	1.386	10.500
1.262	1.500	1.309	6.000		

Figure 1.- Model instrumentation.

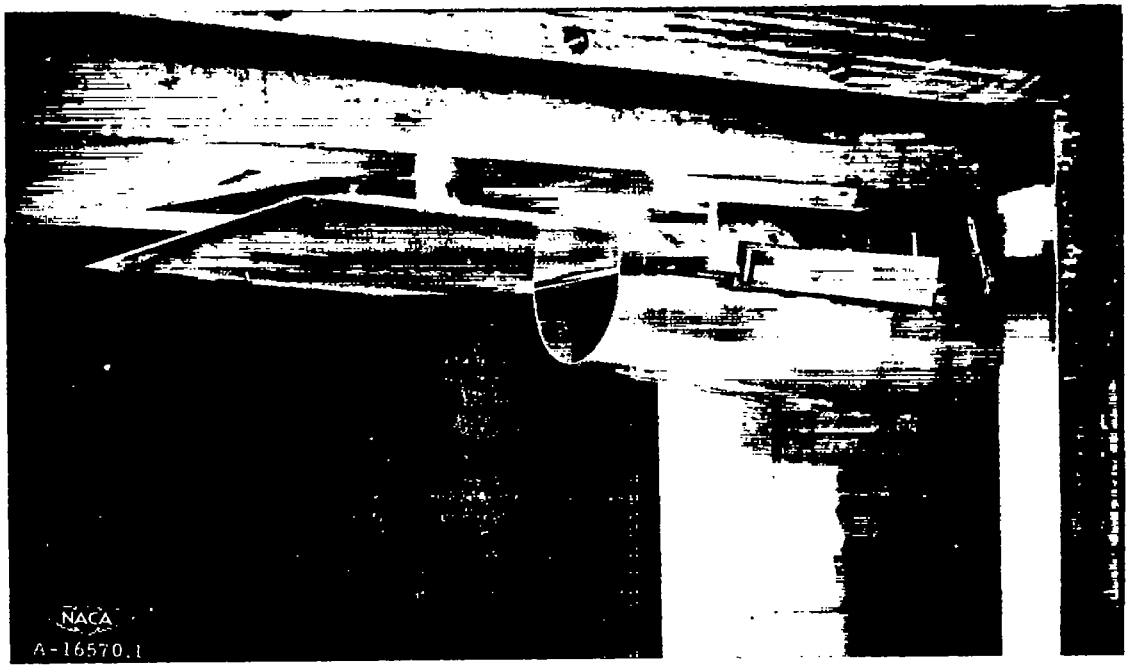

(a) Boundary-layer scoop flush with main inlet.

(b) Boundary-layer scoop extended.

Figure 2.- Photographs of model mounted in wind tunnel.

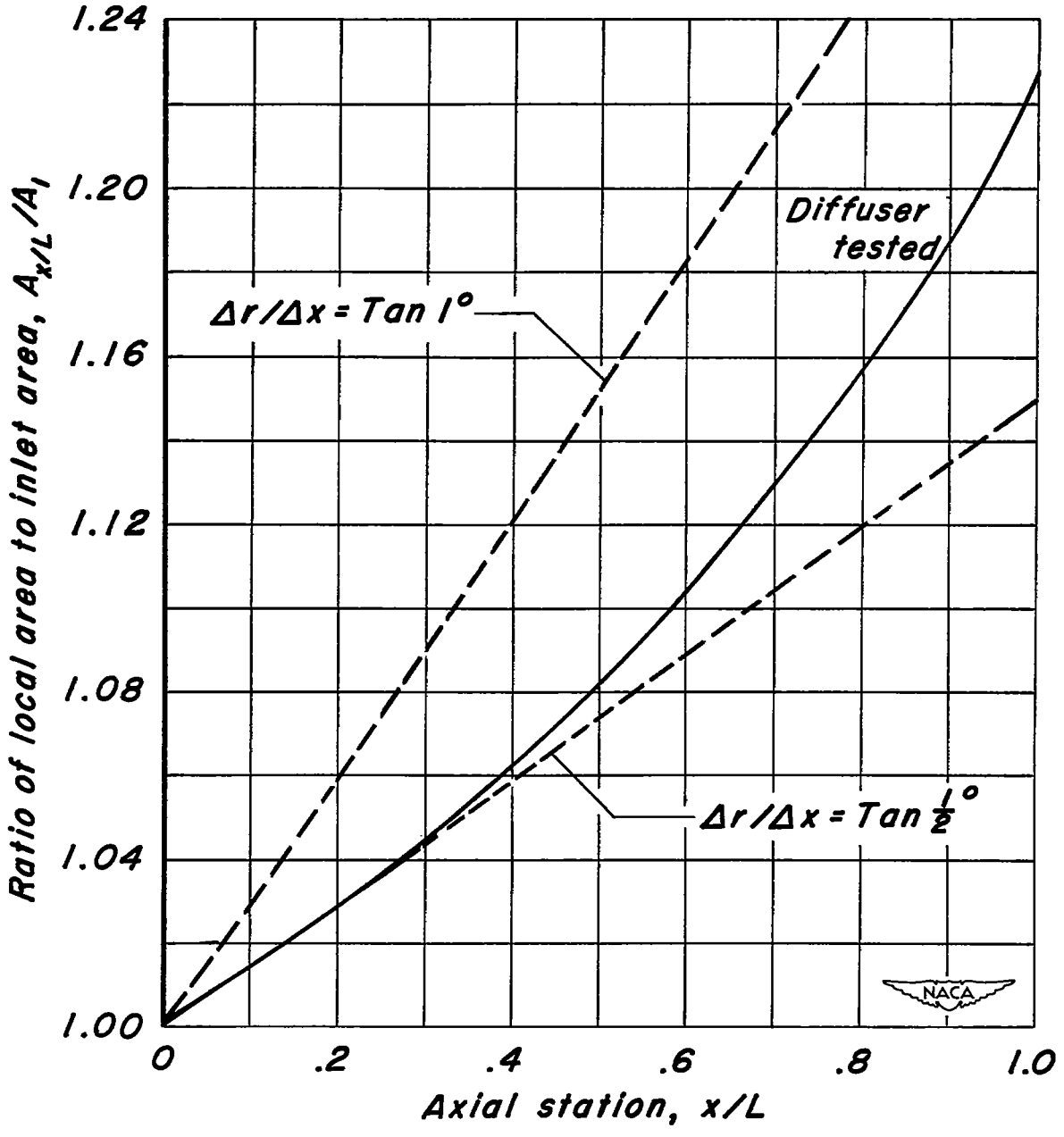

Figure 3.- Variation of duct cross-sectional area.

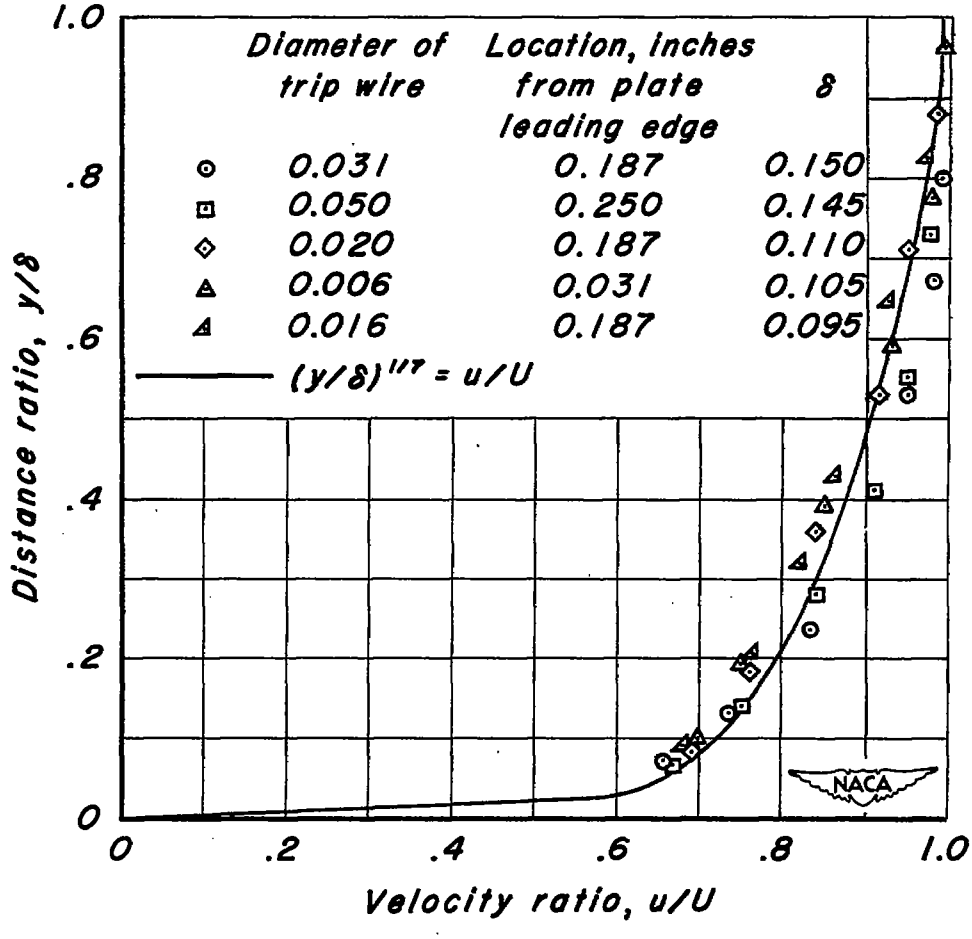

Figure 4.– Dimensionless boundary–layer profiles obtained with trip wires.

[redacted]

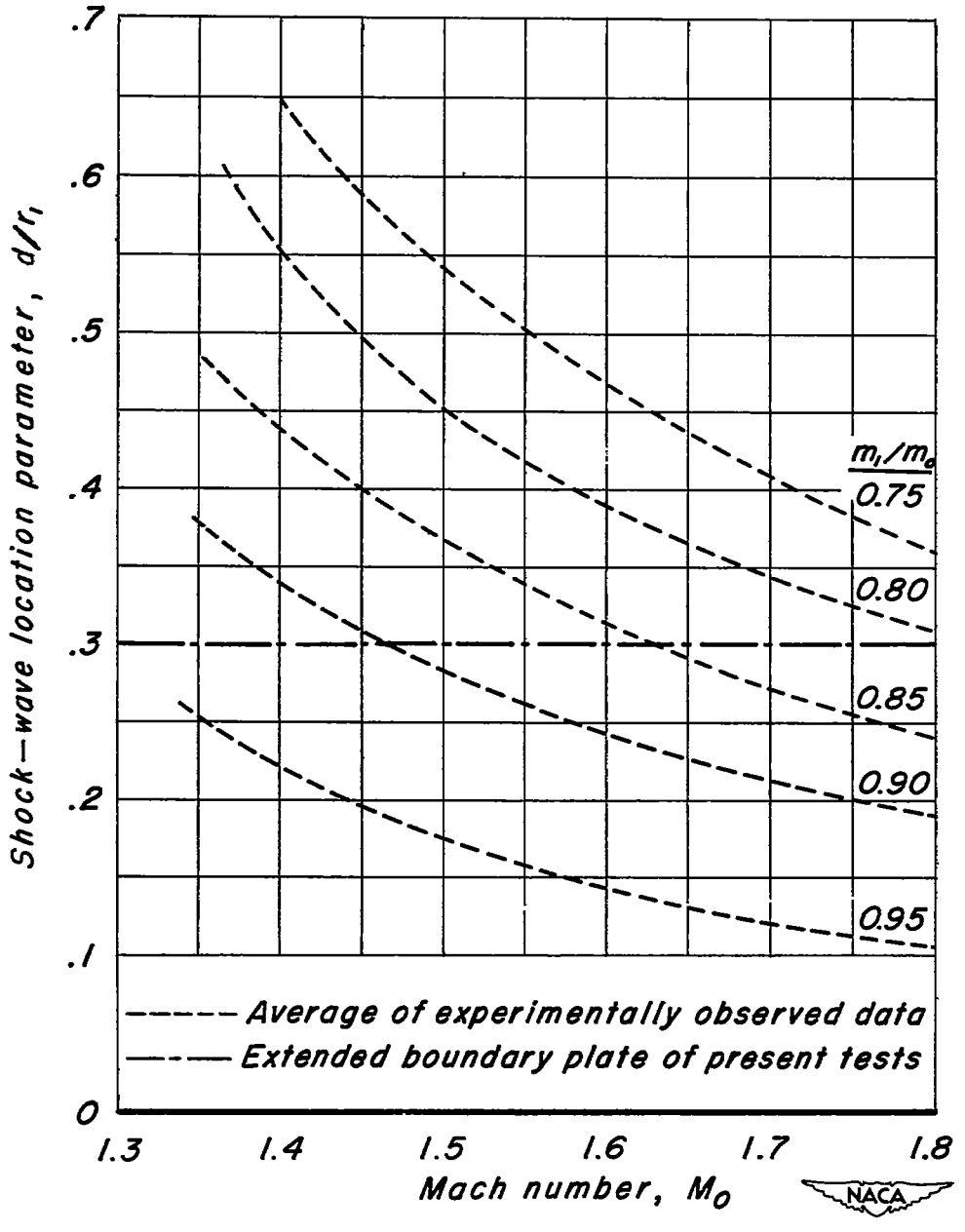

Figure 5.- Effect of Mach number and mass-flow ratio on the external normal-shock-wave location.

[redacted]

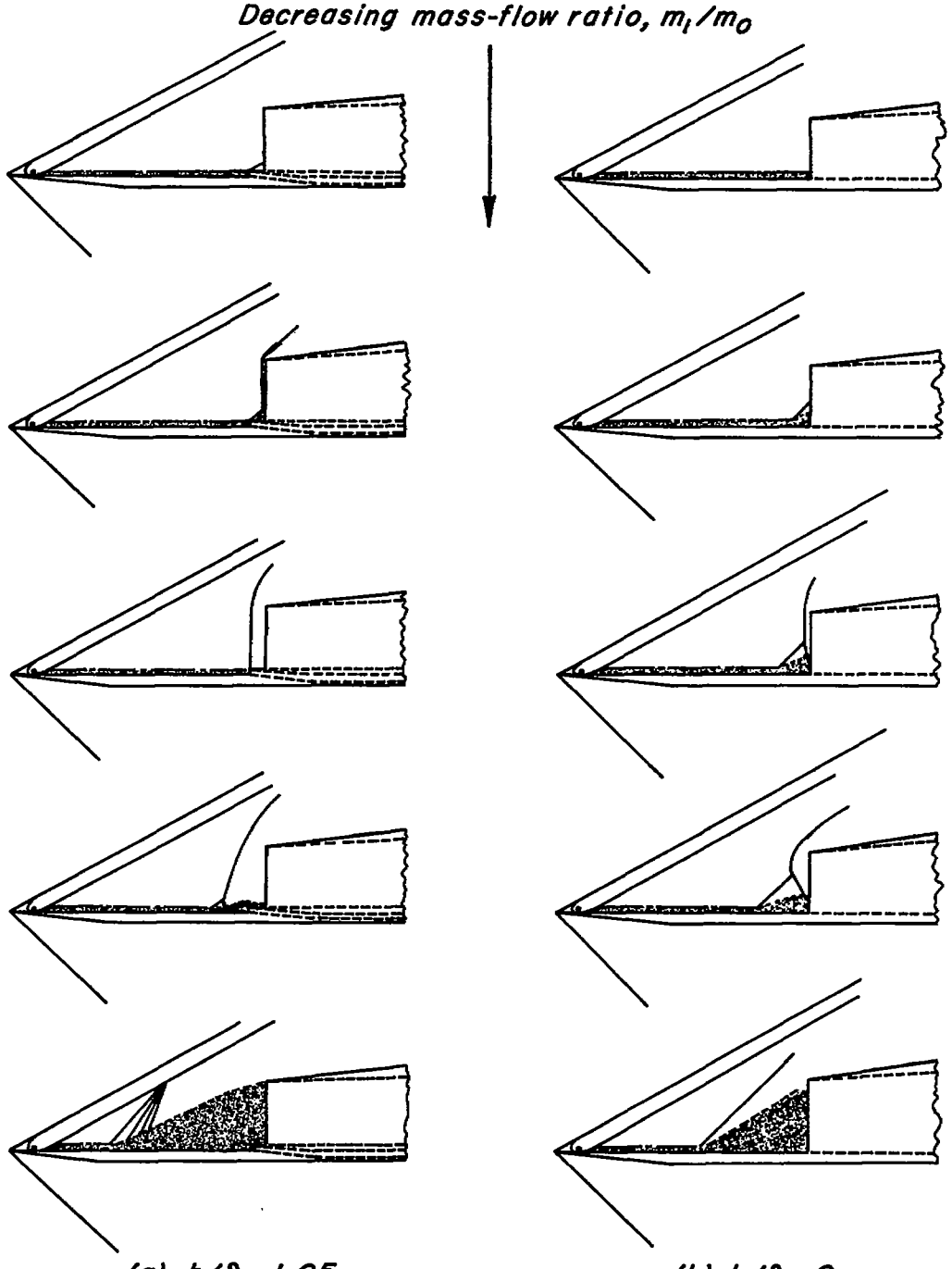

Figure 6. – Sketches of external flow patterns encountered with a decrease in mass-flow ratio at two extreme values of the boundary-layer parameter, h/δ. Flow pattern is typical for all Mach numbers.

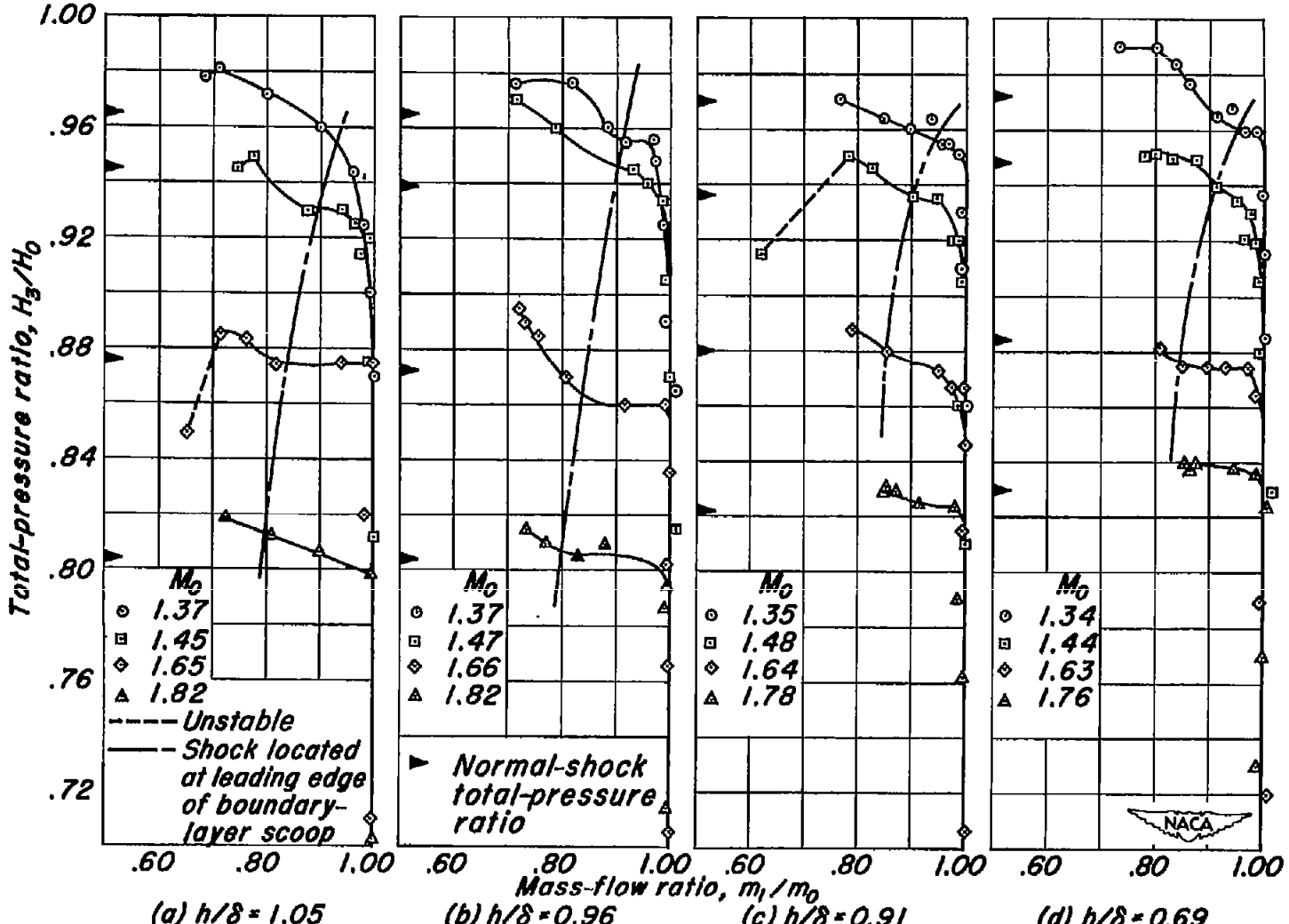

Figure 7.- Total-pressure recovery of the main inlet as a function of inlet mass-flow ratio for various values of the boundary-layer-scoop height parameter and free-stream Mach numbers.

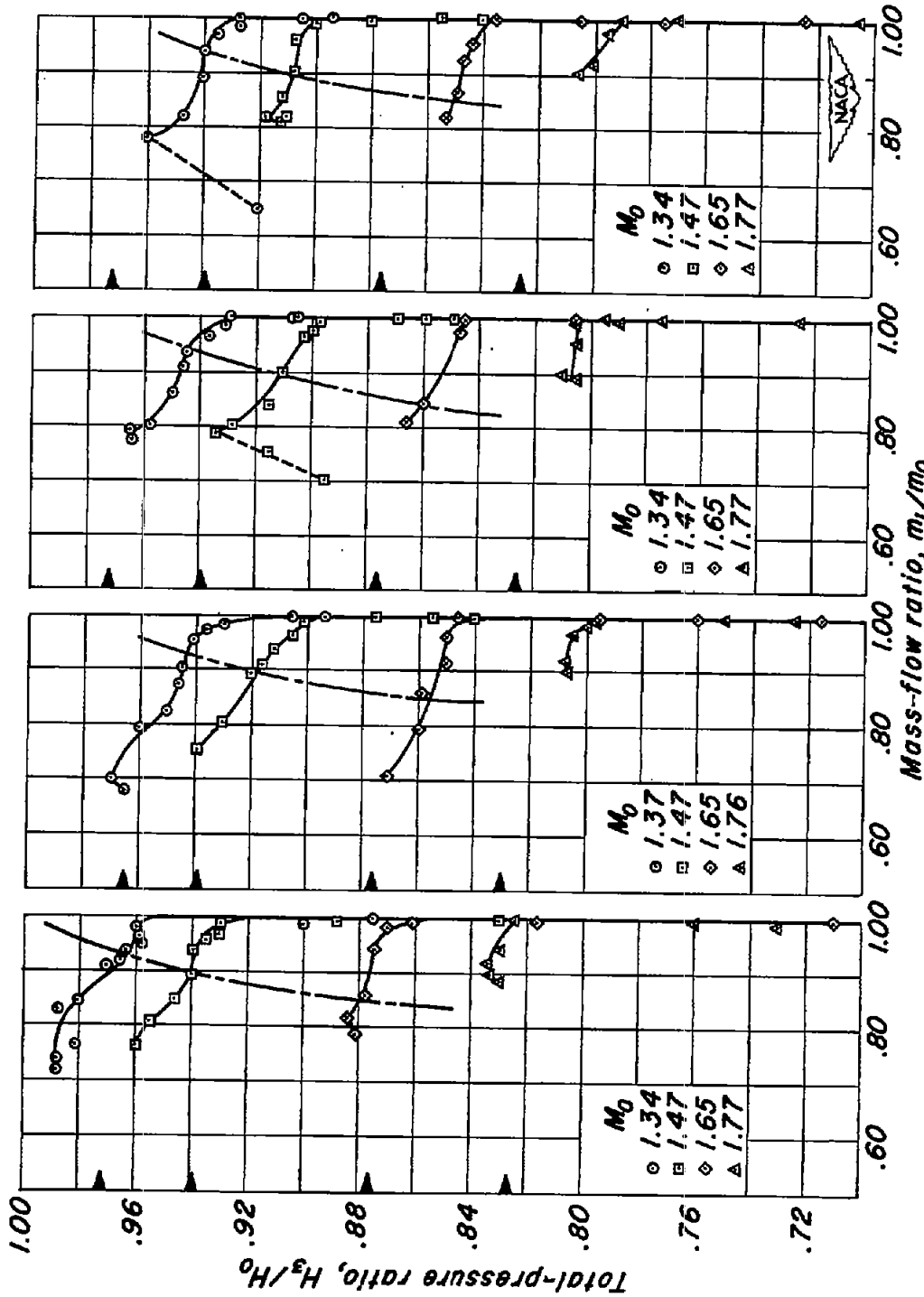

(e) $h/\delta = 0.67$ (f) $h/\delta = 0.61$ (g) $h/\delta = 0.53$ (h) $h/\delta = 0.47$

Figure 7.- Continued.

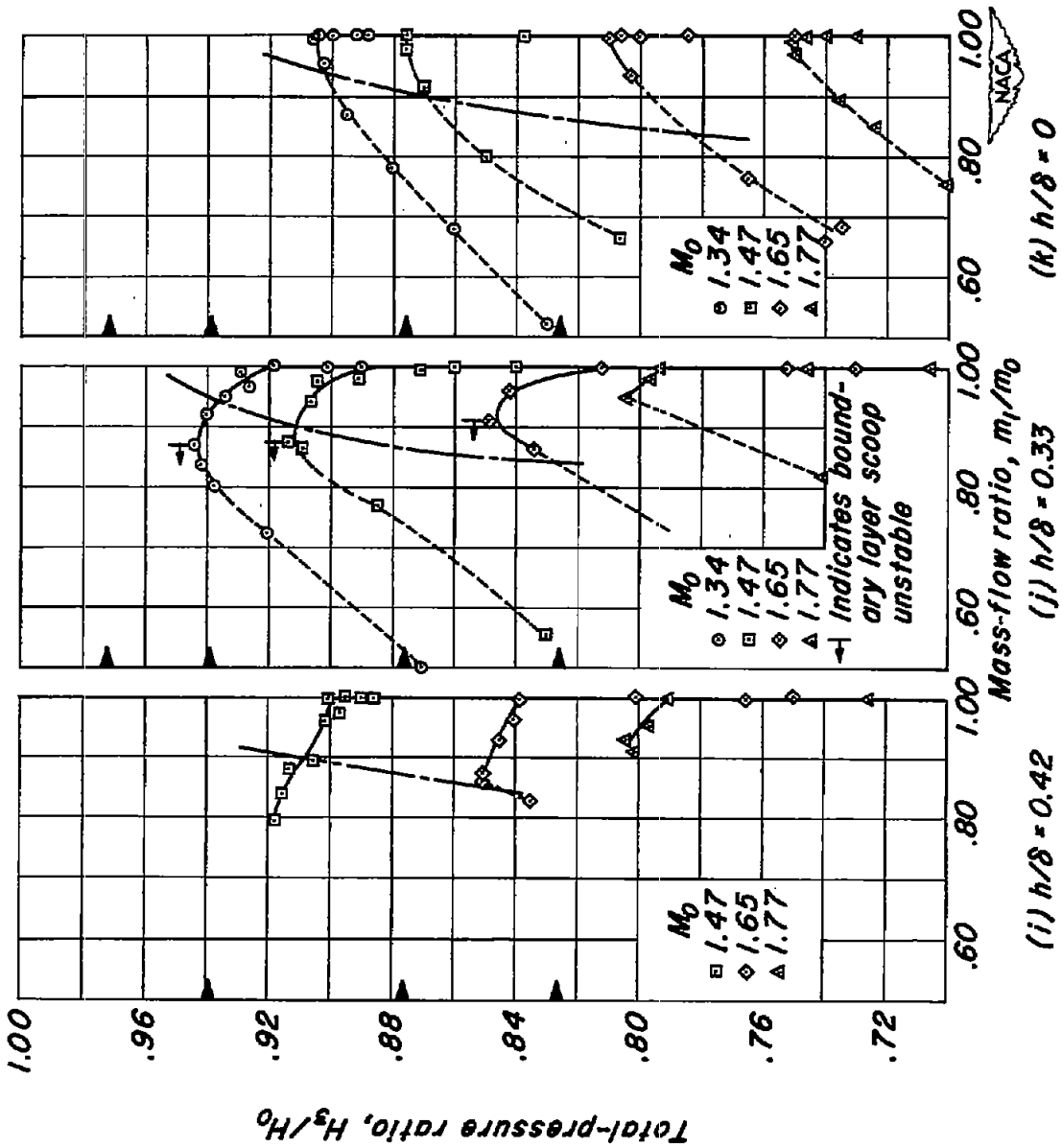

Figure 7.- Concluded.

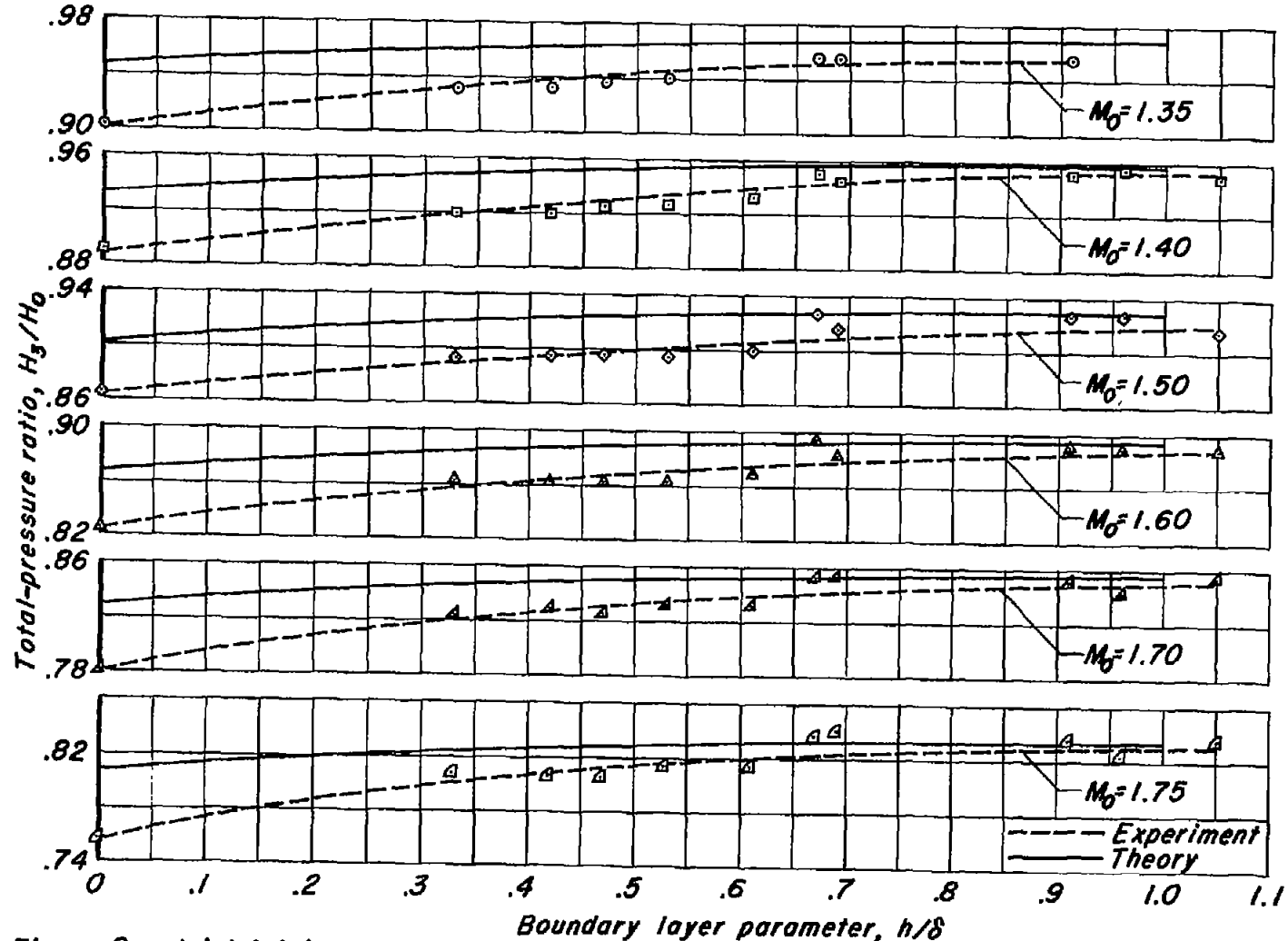

Figure 8.- Inlet total-pressure recovery versus boundary-layer parameter h/δ for a mass-flow ratio of m_1/m_0= 0.95 and for various free-stream Mach numbers.

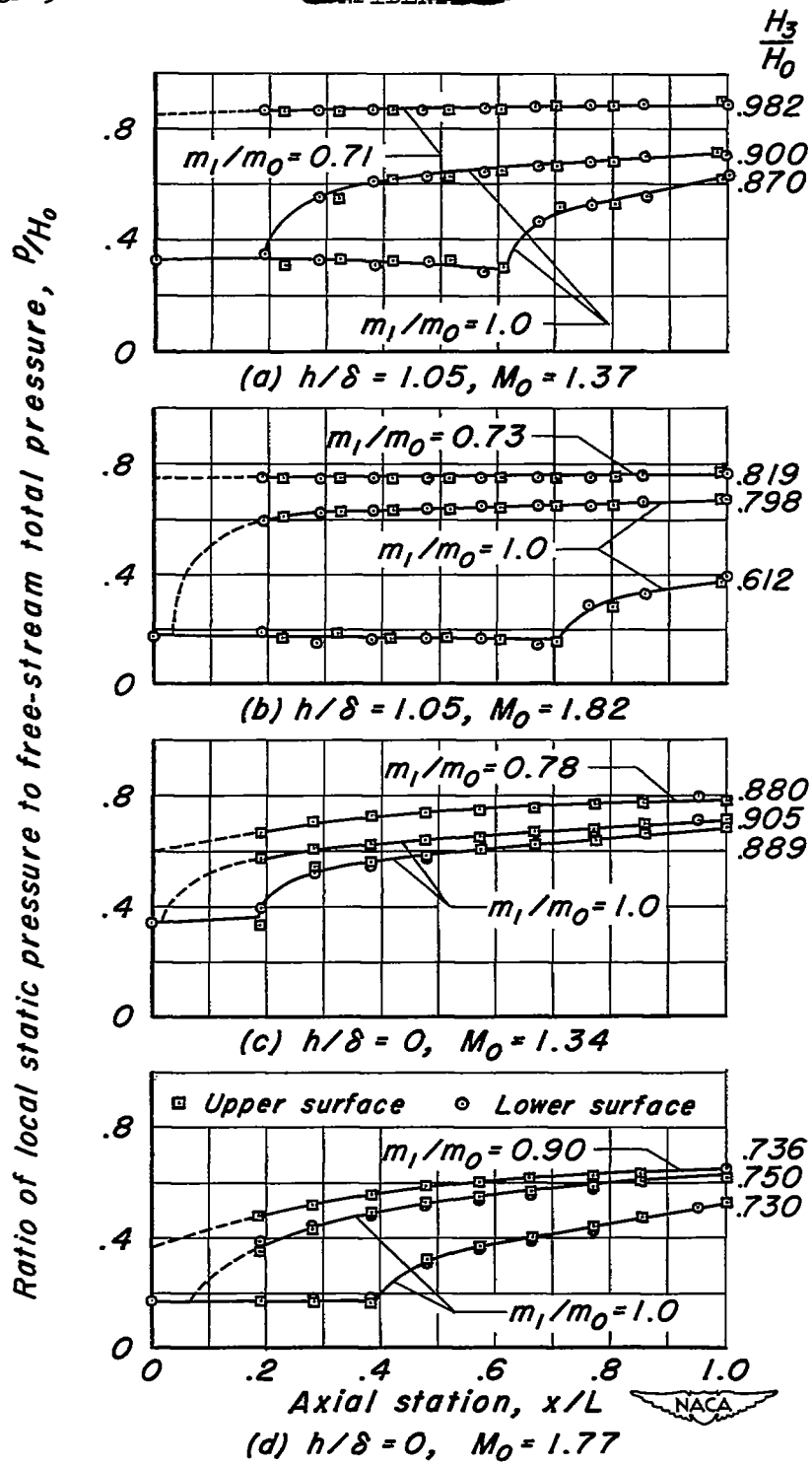

Figure 9.—Internal static-pressure variation at two values of free-stream Mach number and boundary-layer parameter, h/δ.

[redacted]

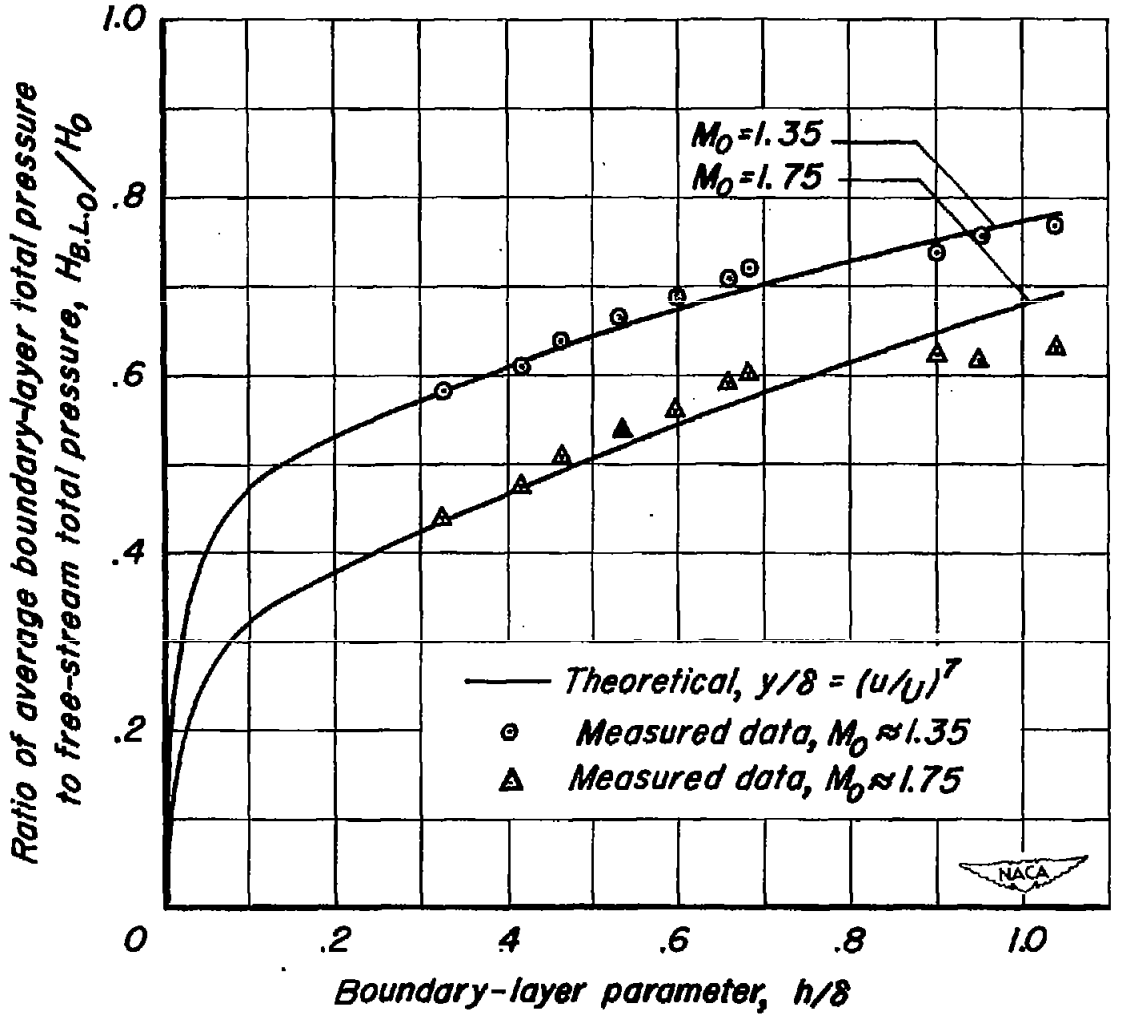

Figure 10.- Ratio of average boundary-layer total pressure to free-stream total pressure as a function of h/δ.

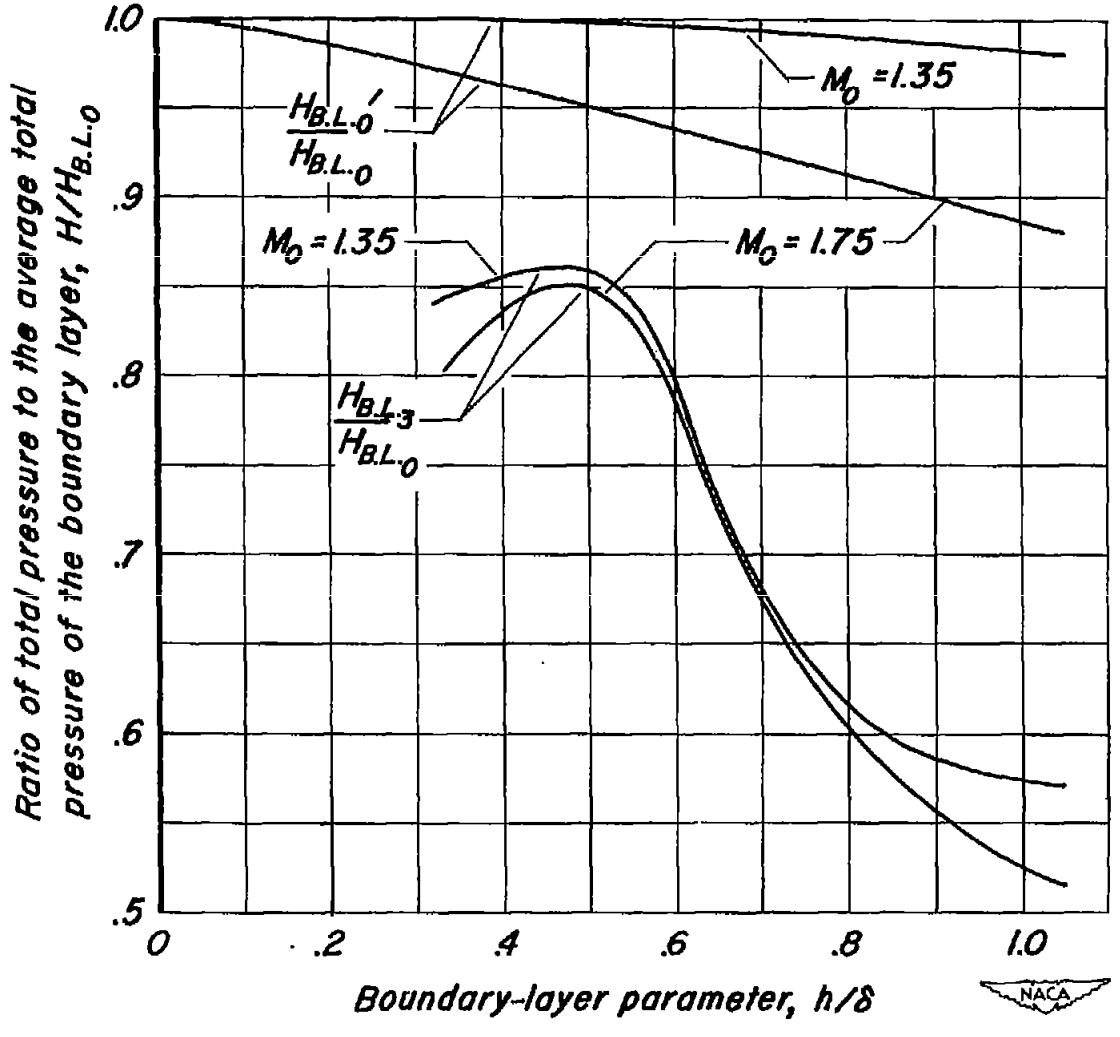

Figure 11.–Ratio of total pressure to the average total pressure of the boundary layer as a function of h/δ.

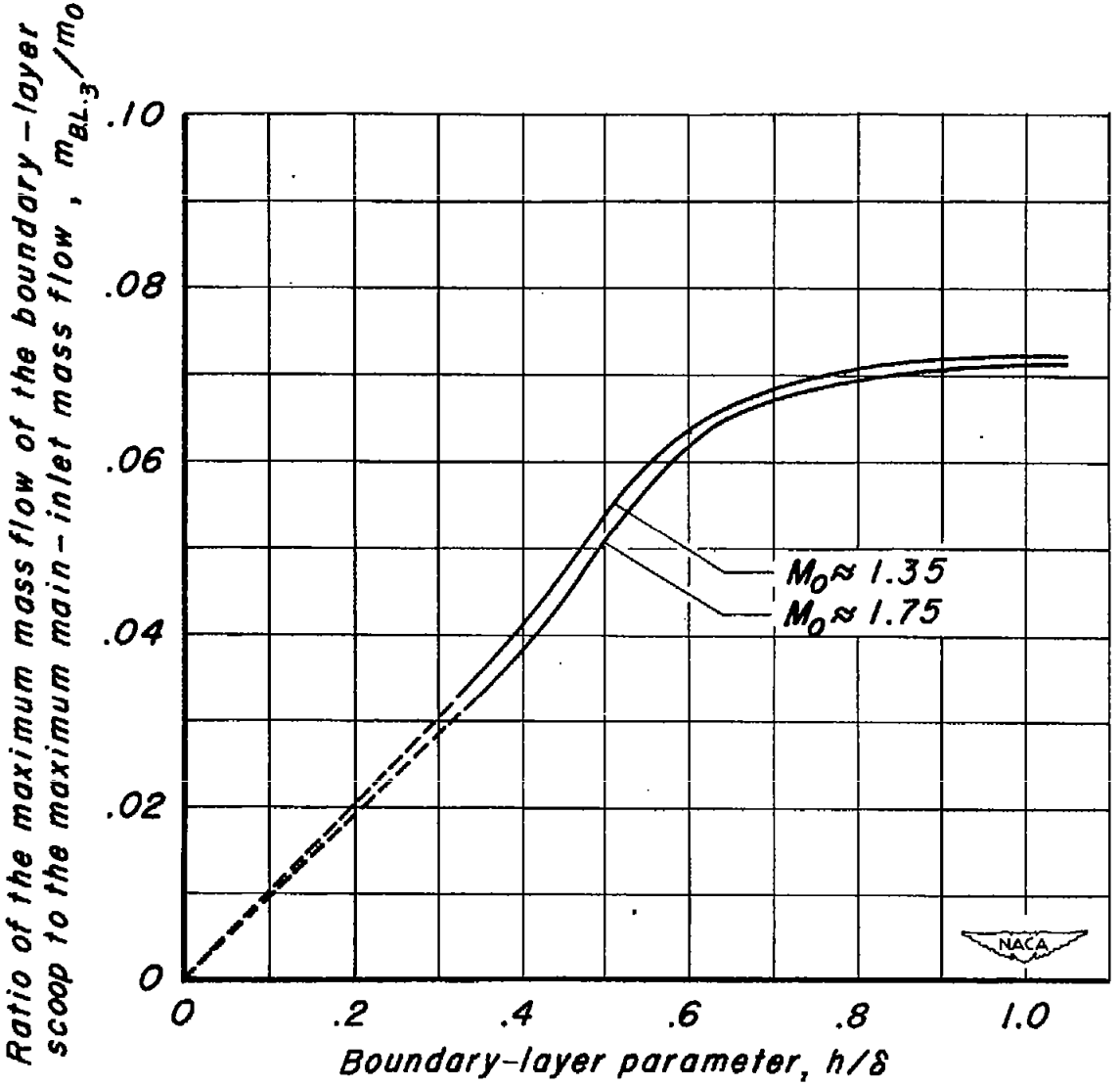

Figure 12.- Ratio of the maximum mass-flow of the boundary-layer scoop to the maximum main-inlet mass flow as a function of h/δ.

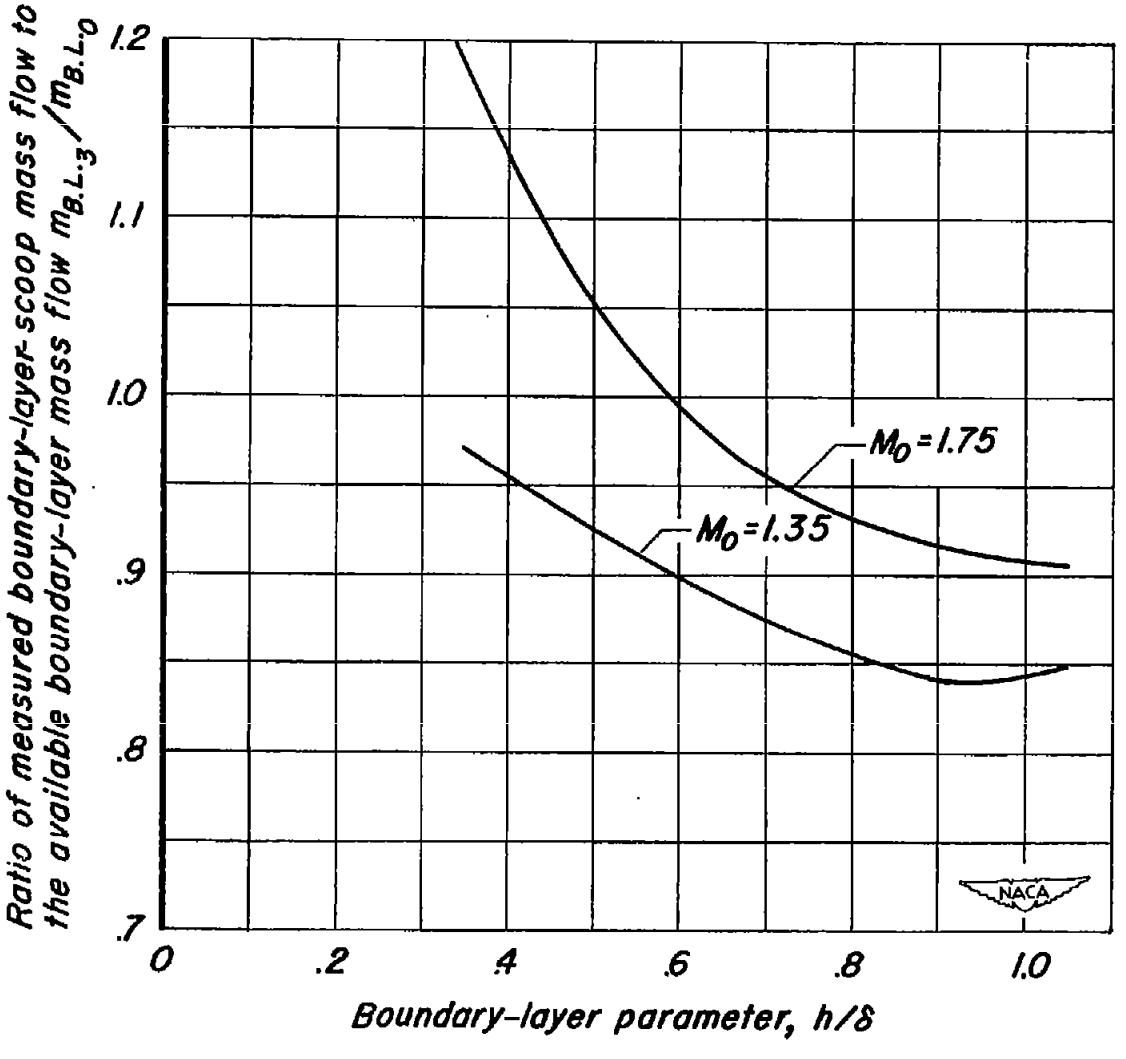

Figure 13.- Ratio of measured boundary-layer-scoop mass flow to the theoretically available boundary-layer mass flow as a function of h/δ.

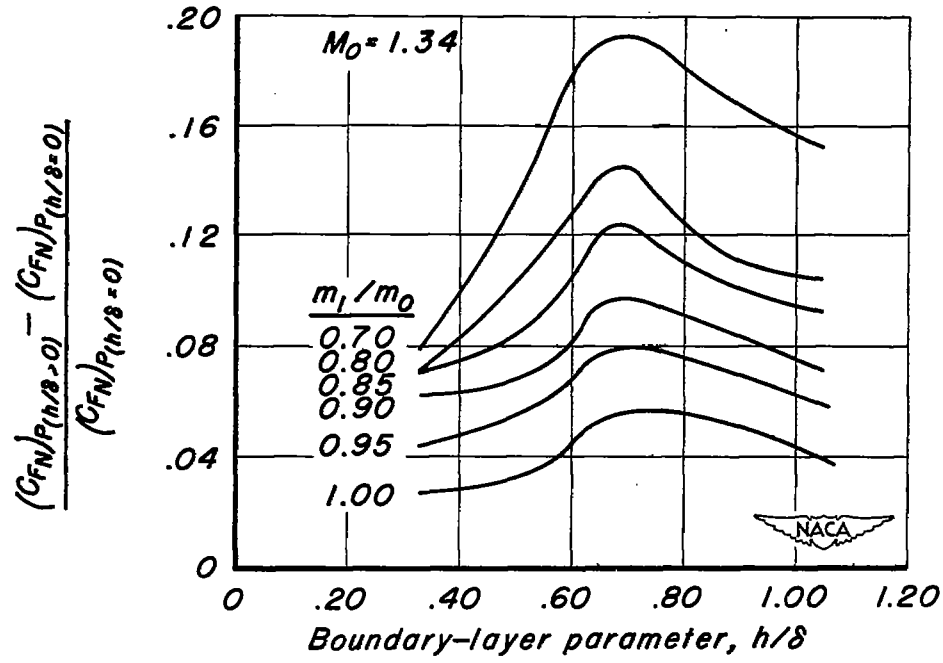

Figure 14.– Relative variation in thrust coefficient due to boundary-layer removal.

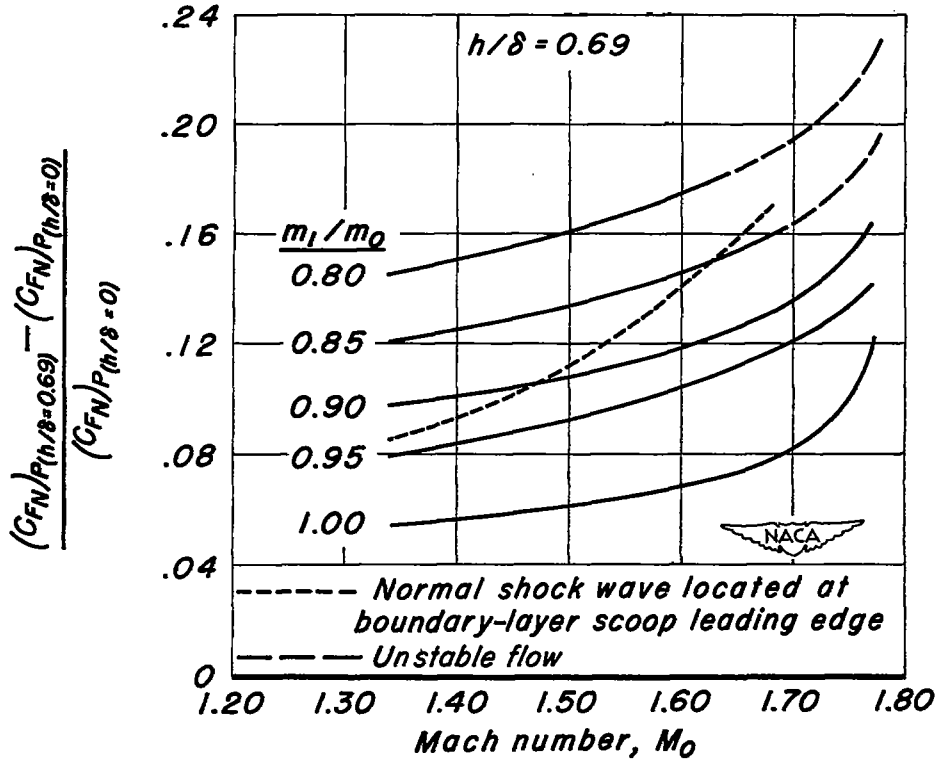

Figure 15.– Relative variation in thrust coefficient with Mach number at optimum boundary-layer removal.

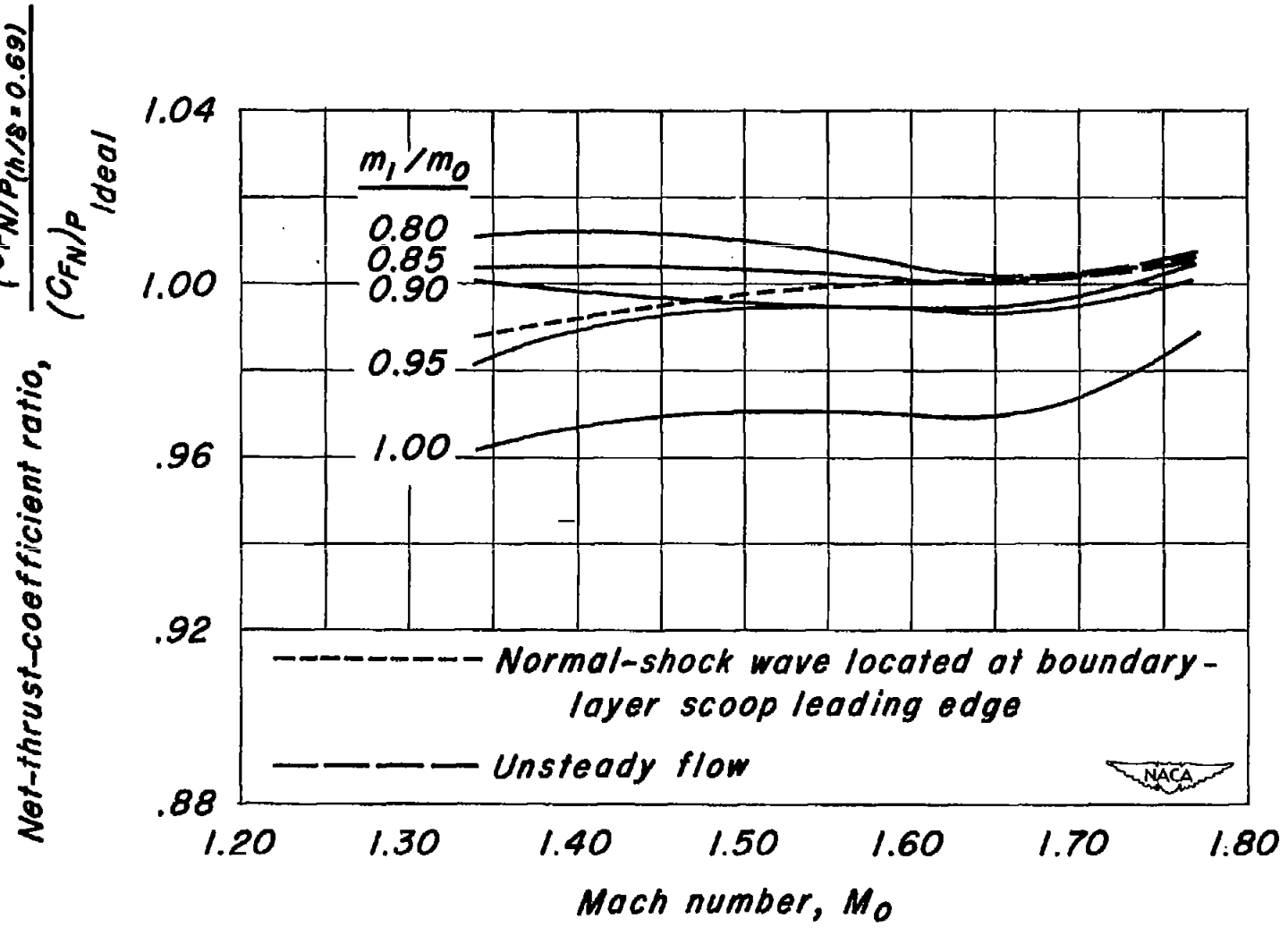

Figure 16.— The effect of Mach number on the net-thrust-coefficient ratio at optimum boundary-layer removal.